Structural, magnetic and thermal properties of one-dimensional $CoFe_2O_4$ microtubes

Zhou-li Lu[1], Peng-zhao Gao[1,2]*, Rui-xue Ma[1], Jia Xu[1], Zheng-he Wang[1], Evgeny V. Rebrov[3]*

[1] College of Materials Science and Engineering, Hunan University, Changsha, 410082, China
[2] Hunan Province Key Laboratory for Spray Deposition Technology and Application, Hunan University China
[3] School of Engineering, University of Warwick, Coventry, CV4 7AL, UK

First corresponding author: Peng-zhao Gao

Email: gaopengzhao7602@hnu.edu.cn Tel: +86 731 88822269; Fax: +86 731 88823554. (Peng-zhao Gao)

Second corresponding author: Evgeny V. Rebrov

E-mail: E.Rebrov@warwick.ac.uk Tel: +44 2476 5 22202

Abstract:

One-dimensional $CoFe_2O_4$ microtubes have been prepared via a simple template-assembled sol-gel method. Influence of calcination temperature on structural and magnetic properties, heat capacity and specific heating rate under radiofrequency field 295 kHz was studied. A $CoFe_2O_4$ spinel was the main phase in all samples. As the calcination temperature increased, the average crystal size increased from 34.1 to 168 nm and the specific surface area decreased from 85.7 to 8.5 $m^2 \cdot g^{-1}$. When calcined at 1073 K, porous microtubes with a narrow size distribution in the range between 2.0 and 2.5 μm and a length to diameter ratio exceeding 20 were obtained. The heat capacity of the microtubes calcined at 973 K was 140.81 $J \cdot mol^{-1} \cdot K^{-1}$ at 395K, being close to the theoretic value. The sample calcined at 973 K showed highest rate of 0.293 K $s^{-1} \cdot mg^{-1}$.

Keywords: Cobalt ferrite; microtubes; magnetic properties; thermal capacity; radiofrequency heating.

1 Introduction

Recently, many researchers have studied different metal oxide morphologies, such as spherical, ordered porous particles, rods, fibers, and hollow structures. The performances of these materials in various applications depend on their chemical composition and surface properties as well as on their textural properties [1-4]. Specially, microtubes play an important role in the miniaturization of components and devices because of their small diameters and high aspect ratios [5]. As their diameter is in the micrometer range, they are more suitable than nanotubes to load guest species such as biomolecules, catalysts, and nanoparticles, which allows to use them in different applications in drug delivery, catalysis, batteries and so on [6]. Currently, hollow metal oxide structures can be prepared with a template method, dry or wet spinning, electrospinning, and centrifugal spinning [7].

Magnetic nanoparticles are the subject of intense research not only for their fundamental scientific interest, but also for their potential applications in magnetic storage media, biosensing applications, catalytic and medical applications [8, 9]. Among the magnetic nanoparticles, spinel cobalt ferrite, $CoFe_2O_4$, is a good candidate due to its high saturation magnetization, high coercivity, strong anisotropy and excellent chemical stability [8]. Spinel type ferrite composites provide a novel platform for system integration in reactor engineering [10, 11]. Ferrite microtubes are promising materials for catalytic applications under radiofrequency (RF) heating due to their highly accessible open structures with large specific surface areas, adjustable Curie temperature and moderate magnetic losses in the kHz range [11]. When embedded into catalytic microparticles, they can be used as susceptors of RF heating [12, 13], which provides efficient and fast heat transfer into catalytic sites and flowing fluid [14-17].

The goal of this study is to develop a method to prepare one dimensional cobalt ferrite microtubes by a template assisted sol-gel synthesis using natural cotton fiber as template. Influence of calcination temperature on the structural and magnetic properties, heat capacity and heating rate in the kHz range of the cobalt ferrites microtubes is presented.

2. Experimental

2.1 Preparation of cobalt ferrite microtubes

Cobalt ferrite microtubes were prepared via a template assisted sol-gel synthesis [18, 19]. Iron (III) nitrate nonahydrate, cobalt (II) nitrate hexahydrate, and citric acid were used as the main raw materials. The metal nitrates were dissolved in ethanol in required molar ratios to prepare solution A. Citric acid was dissolved in ethanol in a separate vessel to produce solution B. Solution B was added into solution A under acutely stir. The resulting mixture was stirred for 4 h and then it was quantitatively titrated by an ammonia solution to a pH of 2.5. The obtained sol was stirred for 24 h then it was absorbed by cotton fibers. These impregnated cotton fibers were dried in an oven at 353 K to get a cobalt ferrite dry gel. The dry gel was calcined at 873, 973, 1073, 1173 and 1273 K for 1 h to produce the corresponding ferrite microtubes. The heating rate during calcination was 2 $K\cdot min^{-1}$ from room temperature to 573 K and then 5 $K\cdot min^{-1}$ from 573 to the desired temperatures followed by a dwelling interval of 1 h at that temperature [18]. The cobalt ferrite microtubes are labeled as CF-T hereafter, where index T represents the calcination temperature in K.

2.2 Characterization of $CoFe_2O_4$ microtubes

The phase composition of the $CoFe_2O_4$ microtubes was determined using an *X*-ray diffractometer (X'Pert PRO) with nickel filtered Cu K_α radiation produced at 40 kV and 27.5 mA, at a scanning rate of

5^o min^{-1} and a step of 0.02^o. The Scherrer equation was used to calculate the average crystal size (*D*, nm), and the $d_{(311)}$ interplanar spacing was determined from the position of the (311) peak using the Bragg equation, also the average lattice constant (*a*) were obtained using Bragg's diffraction condition given by Eq. 1 [20]:

$$\alpha = \frac{\lambda\sqrt{h^2+k^2+l^2}}{2\sin\theta_{hkl}} \quad (1)$$

The specific surface area of $CoFe_2O_4$ microtubes was determined by nitrogen adsorption at 77 K on a Micromeritics NOVA 1000E nitrogen adsorption apparatus.

The Raman spectra of $CoFe_2O_4$ microtubes were recorded in the Raman shift of 160-800 cm^{-1} and carried out on a MKI-2000 spectrometer (Renishaw, UK) with a 532 nm excitation source, equipped with a 1040×256 Renishaw CCD camera, and a laser power of 50mW.

The morphology of $CoFe_2O_4$ microtubes was characterized by scanning electron microscopy (JSM-6700F, Jeol). Transmission electron microscopy was performed with a Tecnan F20 microscope (Philips) operated at 20 kV using the milled powders of $CoFe_2O_4$ microtubes.

The magnetization curves of the as-prepared samples were measured by a vibrating sample magnetometer (Princeton Measurements Corporation MicroMag 3900 VSM) equipped with a 2 Tesla electromagnet.

The specific heat capacity of the $CoFe_2O_4$ microtubes were determined by a STA 449C TG-DSC Analyser (Netzsch Thermische Analyser, Germany) fitted with an appropriate software. The samples (10 mg) were placed in platinum pans that were closed and heated under nitrogen flow of 60 mL/min from 305 to 575K at a heating rate of 5 K/min. Prior to the measurements, the instrument was calibrated under the same experimental conditions, with a sapphire disk (weight: 25.93 mg) [21]. The recommended sapphire reference heat capacity data from the NIST database was used to adjust the results according to Eq. 2 [22, 23]:

$$\frac{C_{p,sam}}{C_{p,\ std}} = \frac{H_{sam} - H_{bsl}}{M_{sam}} \div \frac{H_{std} - H_{bsl}}{M_{std}} \qquad (2)$$

where, $C_{p,}$ is the molar heat capacity, M is the sample weight, H is the heat effect. Subscripts bsl, std, sam are referred to an empty vessel, the standard sample (sapphire disk) and the ferrite sample, respectively.

The specific heating rates of the $CoFe_2O_4$ microtubes were measured at a frequency of 295 kHz. The sample was placed in a quartz tube inserted along the center axis in a 50 mm RF coil connected to an Easy Heat RF system (Ambrell) operated at a current of 200 A. Prior to the measurements, a slurry of ferrite (10mg) in deionized water (80 mg) was made to enhance heat transfer towards the temperature sensor. The slurry temperature was measured with a fiber optic sensor (FISO). The specific heating rate was calculated from the initial (linear) part of temperature vs time curves taken into account the specific heat capacities of the ferrite and water in the slurry and their weight fractions.

3. Results and discussion

3.1 Effect of calcination temperatures on the structural properties of the $CoFe_2O_4$ microtubes

Figure 1 shows XRD spectra of $CoFe_2O_4$ microtubes calcined at different temperatures. The sample calcined at 873 K has amorphous structure. A spinel phase is formed in the 973-1273 K range. The peaks are indexed with the standard pattern reported in JCPDF cards (#22-1086 for $CoFe_2O_4$). Below 1173 K, all samples show a sharp diffraction peak at 35.437^o 2 theta, which is ascribed to the (311) plane. However, other peaks are rather wide which indicates that the obtained material has low degree of crystallinity [18].

Also, a minor amount of impurity, cubic Fe_2O_3, (labeled as A in Figure 1) is detected when calcination temperature is below 1073K. The presence of the cubic Fe_2O_3 phase can be explained by small discrepancies in molar ratios of metal nitrates or the segregation of metal oxides during the drying step. As the calcination temperature increases, the content of impurity gradually decreases and finally disappears at 1173K.

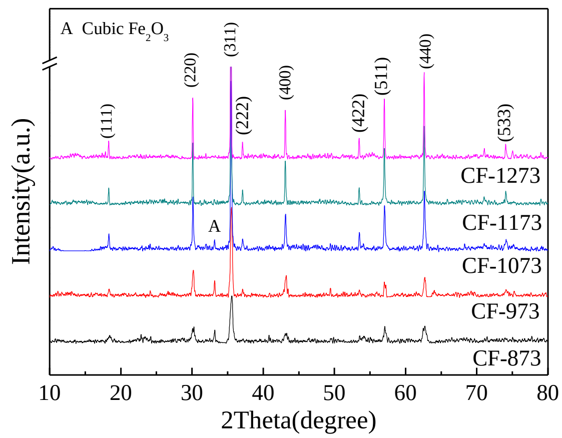

Figure 1. XRD patterns of $CoFe_2O_4$ microtubes calcined at different temperatures.

Insert Figure 1 here

The average crystal size, interplanar spacing (d_{311}) and specific surface area of the microtubes calcined at different temperatures are listed in Table 1. It can be seen that the specific surface area decreases by a factor of nearly eight as the calcination temperature increases from 873 to 1273 K due to progressive aggregation of small crystallites into larger particles. When calcined at 1073 K, the average crystal size and the specific surface area are 66.9 nm and 46.5 $m^2 \cdot g^{-1}$, respectively. The latter value is nearly 10 times higher than that previously reported for Co ferrites [24]. This indicates that the template-assisted sol-gel method can improve the specific surface area of the ferrites though it slightly increases the average crystal size at the same time. This is mainly due to the fact that highly porous structure is obtained in the template assisted method. As the calcination temperature increases, the d_{311} interplanar spacing approaches the value for the bulk $CoFe_2O_4$ material.

Insert Table 1 here

Table 1. Physical properties of $CoFe_2O_4$ microtubes calcined at different temperatures.

Samples	CF-873	CF-973	CF-1073	CF-1173	CF-1273
Average crystal size (nm)	A	34.1	66.9	123	168
Interplanar spacing (d_{311} nm)*	A	2.5228	2.5267	2.5289	2.5292
Specific surface area ($m^2 \cdot g^{-1}$)	85.7	69.8	46.5	13.4	8.5
Cell parameters α (nm)	A	0.837	0.838	0.839	0.839

A – Amorphous

*standard d_{311} interplanar spacing of $CoFe_2O_4$ is 2.531 nm and unit cell parameters is 0.839 nm.

3.2 Raman spectra study of the $CoFe_2O_4$ microtubes

It is known that $CoFe_2O_4$ has a cubic inversed (or mixed) ferrite structure with a O_h^7 symmetry (Fd3m space group), which gives rise to 39 normal vibrational modes, out of which five are Raman active [25, 26].

$$A_{1g} + E_g + 3T_{2g} \qquad (3)$$

Lattice distortion, local cation distribution and magnetic ordering can be determined by Raman spectroscopy [25]. Figure 2 shows room temperature Raman spectra of the $CoFe_2O_4$ microtubes calcined at different temperatures. Five peaks with maxima near 684, 609, 466, 301, and 200 cm^{-1} are observed in all **s**pectra. The tetrahedral breath modes at 684 and 609 cm^{-1} are assigned to symmetric stretching vibrations of oxygen atoms with respect to a metal ion in the tetrahedral void [25]. The other low frequency peaks are assigned to vibrations of metal ions in octahedral voids, i.e., E_g and T_{2g} [27]. These modes correspond to the symmetric and anti-symmetric bending vibrations of oxygen atom in the M–O bond in the octahedral voids [28]. The positions of the peaks are in line with the previously reported data [25, 29]. Our data confirm that all as-synthesized samples are $CoFe_2O_4$ with a cubic inverse-spinel structure. As the calcination temperature increases, the peaks shift to higher frequencies (Table 2) due to increased crystallite size [27]. The relative intensity of the peaks remained constant, indicating cation redistribution did not occur in the $CoFe_2O_4$ microtubes at higher calcination temperatures.

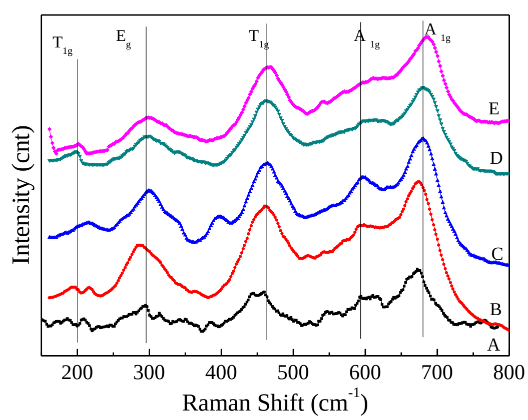

Figure. 2 Raman spectra of $CoFe_2O_4$ microtubes calcined at different temperatures.

A: CF-873, B:CF-973, C: CF-1073, D: CF-1173, E: CF-1273

Insert Figure 2

here

Insert Table 2 here

Table 2. Positions of the peaks in the Raman spectra of the $CoFe_2O_4$ microtubes calcined at different temperatures[25,26]

Sample	Raman shift (cm^{-1})				
	A_{1g} (1)	A_{1g}(2)	T_{1g}(1)	E_g	T_{1g}(2)
CF-873	675	594	460	294	187
CF-973	675	597	463	289	194
CF-1073	680	597	464	300	-
CF-1173	682	607	464	301	199
CF-1273	684	609	466	301	200
Reference	[25]	[25]	[25]	[25]	[25, 29]

3.3 Effect of calcination temperature on the microstructure of $CoFe_2O_4$ microtubes

Figure 3 shows characteristic SEM images of the $CoFe_2O_4$ microtubes. It can be seen that one-dimensional isolated microtubes are obtained in the template-assembled sol-gel method. Their morphology, diameter as well as the ratio of length to diameter can be changed by increasing calcination temperature. The template consists of isolated fibers with a predominantly parallel orientation (Figure 3(a)). The individual fibers exhibit axial and vein-liked texture with a diameter about 25 μm (Figure 3(b)). The most of microtubes have a length exceeding 50 μm and they are separated from each other (Figure

3(c)). Calcination at 873 K results in amorphous microtubes with a mean diameter of 3-4 μm and a small number of individual crystals (Figure 3(d)). When calcined at 1073 K, the porous microtubes with a diameter in the range from 2 to 2.5 μm and an aspect ratio above 20 are produced. They consist of rather uniform particles with a size about 80 nm (Figure 3(e)). Calcination at 1273 K results in larger particles exceeding 180 nm while the microtube diameter decreases to 2.0 μm (Figure 3(f)).

Insert Figure 3 here

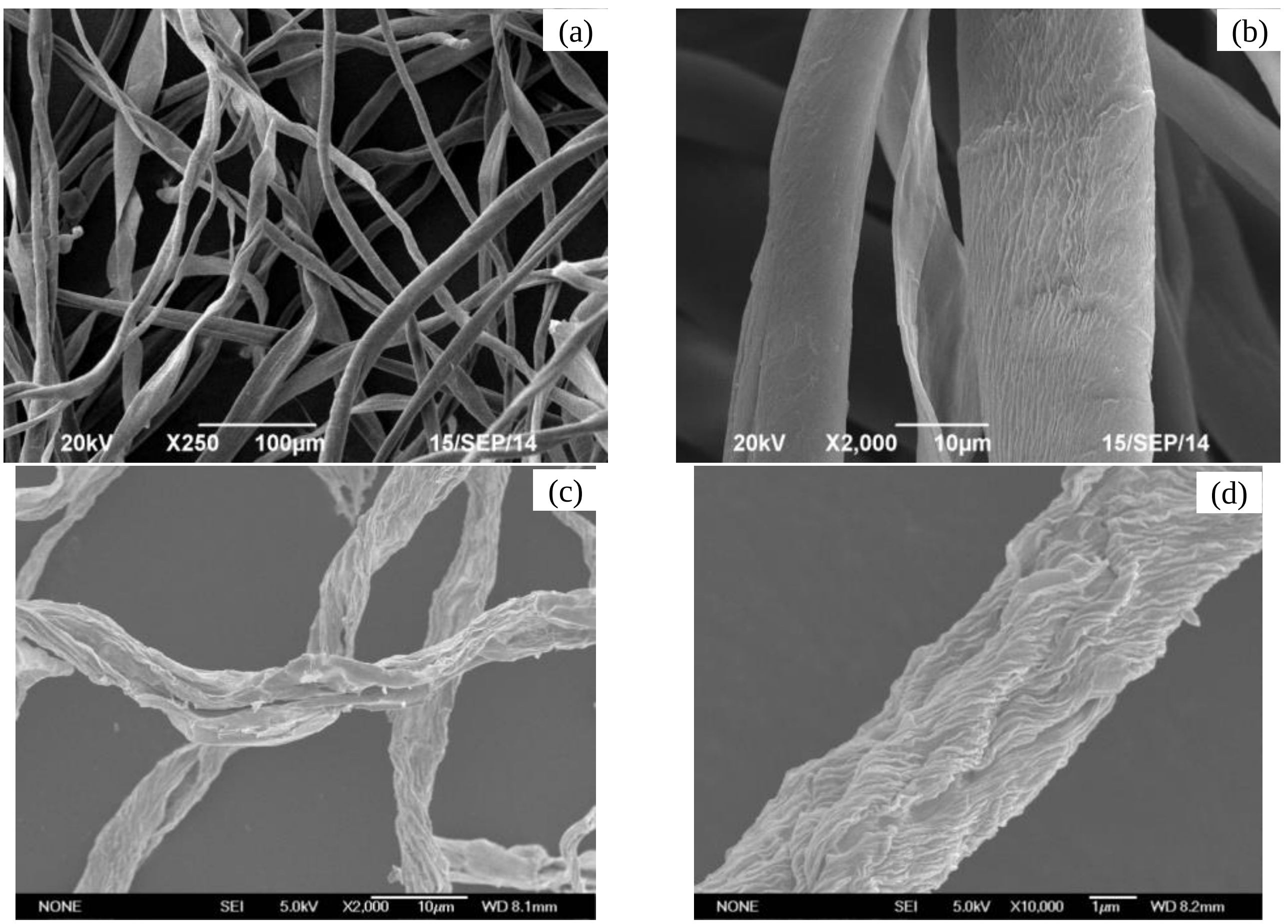

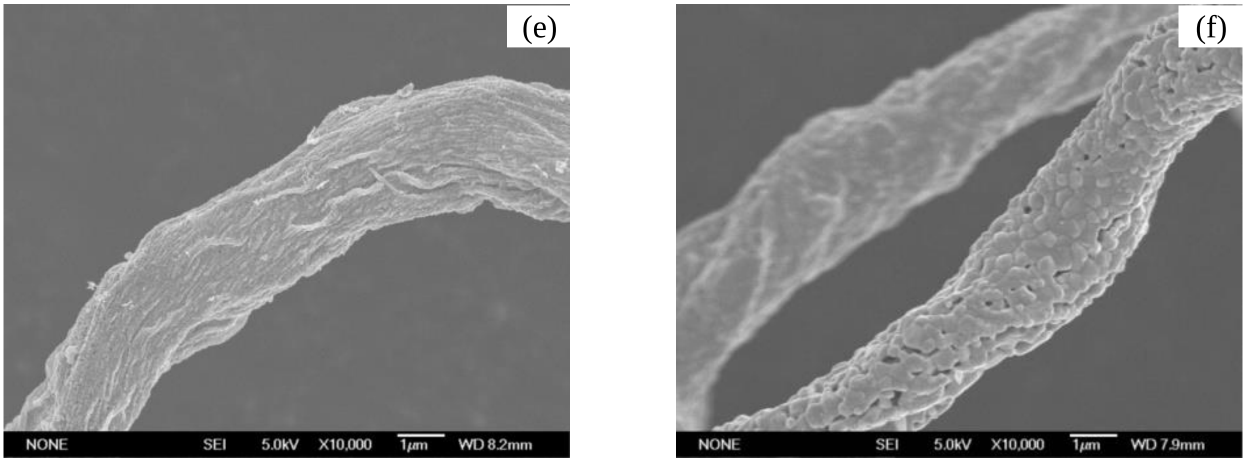

Figure 3. SEM images of CF templates and $CoFe_2O_4$ microtubes calcined at different temperatures. (a) Cotton fiber; (b) Cotton fiber at larger magnification, (c) CF-873, (d) CF-873 at larger magnification, (e) CF-1073, (f) CF-1273.

TEM images show that the $CoFe_2O_4$ microtubes are formed by individual nanoparticles (Figure 4). The particles form irregular polyhedrons with mean sizes between 20 and 120 nm that are connected by necks. The magnetic attraction force is responsible for agglomeration of particles during calcination and results in this specific shape. As the calcination temperature increases, the amount of amorphous phase decreases and the nanoparticle size increases.

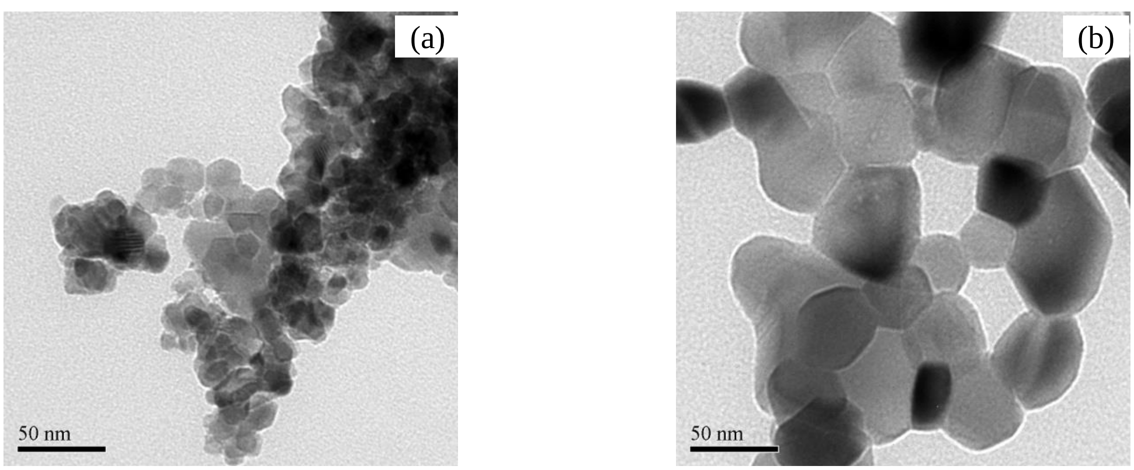

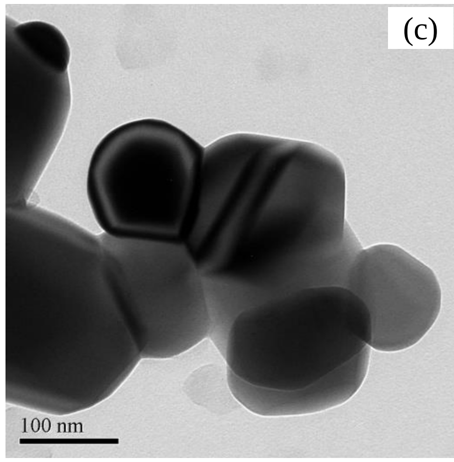

Figure 4. TEM images of $CoFe_2O_4$ microtubes calcined at different temperatures
(a) CF-873; (b) CF-1073; (c) CF-1273

Insert Figure 4 here

3.4 Effect of calcination temperature on the magnetic properties of $CoFe_2O_4$ microtubes

Room temperature hysteresis loops for the $CoFe_2O_4$ microtubes calcined at different temperatures are shown in Figures 5(a) and (b) and their magnetic parameters are listed in Table 3.

Insert Figure 5 here

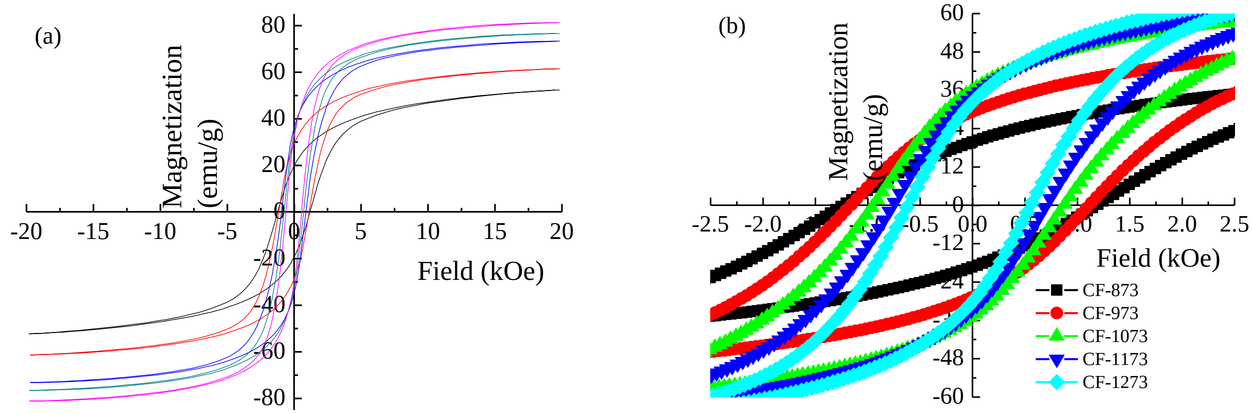

Figure 5. Magnetization curves of $CoFe_2O_4$ microtubes calcined at different temperatures

(a) external field ranged between -20 and 20kOe; (b) external fields ranged between -2.5 and 2.5kOe

As the calcination temperature increases from 873 to 1073 K, the saturation magnetization increases, the coercivity monotonously decreases while the Curie temperature remains rather constant. The remnant magnetization first increases and then decreases (Table 3).

It is known that the saturation magnetization in nanoparticles is influenced by both the intrinsic and extrinsic factors [30-33]. The former are composition, preferential site occupancy of the cations, exchange effect, while the latter are microstructure and grain size. The samples with low degree of crystallinity obtained at relatively low calcination temperatures have a high defect density and a higher proportion of surface to internal atoms. In these samples, a relatively larger number of surface atoms is responsible for a disordered state of magnetic moment. Therefore they cannot be easily magnetized when applying an external magnetic field. On the other hand, the existence of defects also hinders the rotation of atomic magnetic moments to the external field direction during the magnetization process. These two factors lead to a lower saturation magnetization. As the calcination temperatures increases, both the particle size and crystallinity increase. This reduces the influence of the thermal disturbance of the surface atoms on the magnetic moment. The magnetic structure becomes more ordered, resulting in a higher saturation magnetization [34]. The exchange interaction between the cobalt ferrite phase and impurity in ferrites decreases as the amount of impurity gradually decreases and finally disappears at higher calcination temperatures. This results in a decrease of the saturation magnetization [30, 35]. Namely, with the increase of calcination temperatures, the variety of particle size and degree of crystallinity would always result in an increase of the saturation magnetization while the exchange interaction in its decrease [32, 35]. It appears that the combined effect of exchange interaction and crystal size levels out a monotonous increase of saturation magnetization in these samples.

Insert Table 3 here

Table 3. Magnetic properties of $CoFe_2O_4$ microtubes calcined at different temperatures.

Sample	CF-873	CF-973	CF-1073	CF-1173	CF-1273
Saturation magnetization (emu/g)	52.3	61.4	73.3	76.6	81.2
Remnant magnetization (emu/g)	19.6	29.0	35.4	33.3	31.2
Ratio of M_r/M_s	0.37	0.47	0.48	0.44	0.38
Coercivity (Oe)	1208	1137	910	731	586
Curie temperature (K)	803	798	798	798	803
$\varepsilon_p \times 10^{-5}$ (erg/cm^2)	A	0.12	0.12	0.12	0.12
Critical particle size (nm)	A	44.0	30.9	28.3	25.2

A – Amorphous

The coercivity of magnetic materials is mainly affected by particle size, magnetic anisotropy, stress anisotropy and magnetic domain structure [36]. As for cobalt ferrite, anisotropy is mainly provided the incompletely quenched orbital angular momentum of the Co^{2+} ions. As the calcination temperature increases, the anisotropy constant of Co^{2+} decreases, which decrease the coercivity of cobalt ferrite. The transition from single to multidomain region occurs at a critical particle size which was estimated by Eq. 4 [37]. The critical particle sizes are listed in Table 3.

$$d_{cr} = \frac{9\varepsilon_p}{2\pi M_s^2} \qquad \text{(in CGS units)} \tag{4}$$

where M_s is the saturation magnetization and ε_p is the surface energy of the domain wall calculated by Eq. 5 [38].

$$\varepsilon_p = \left(\frac{2k_B T_C K_1}{a}\right)^{0.5} \tag{5}$$

where k_B is the Boltzmann constant (1.38×10^{-16} erg·K^{-1}), T_c the Curie temperature, a is the lattice parameter, and K_1 is the absolute value of magnetocrystalline anisotropy constant. The anisotropy constant only slightly changes with composition [37, 38], therefore K_1 was assumed to be constant and equal to 5.10 $\times10^4$ erg/cm^2 [36, 39].

A comparison of average crystal size (Table 1) and critical size (Table 3), suggests that all cobalt ferrite samples have a multidomain structure. Their coercivity is inversely proportional to the grain size [40, 41] (Eq. 6).

$$H_c = p_c \frac{\sqrt{AK_1}}{M_s D} \tag{6}$$

where p_c is a dimensionless factor, A is the exchange constant. The coercivity data (Table 3) agreed well with predictions of Eq.6. The remnant magnetization reaches the maximum value of 35.42 emu/g in the sample calcined at 1073 K. This is in line with the data previously reported by Ma [42].

3.5 Heat capacity measurements of $CoFe_2O_4$ microtubes

The isobaric molar heat capacity ($C_{p,m}$) of $CoFe_2O_4$ microtubes was measured in the 308 – 573 K temperature range (Figure 6). The $C_{p,m}$ data were fitted by a second order polynomial function [21]:

$$Cp = A + B\times T + C\times T^{2} \tag{7}$$

The parameter values are listed in Table 4. Weak temperature dependence of the samples calcined at higher temperatures is due to improved crystallinity in samples. The Kopp's law can be used to calculate the specific heat capacity of $CoFe_2O_4$ (Eq. 8) [43]:

$$C_v = \sum n_i C_{v,i} \tag{8}$$

where n_i is the atomicity of element *'i'* in compound, and $C_{v,i}$ is the specific heat capacity of element *'i'* in compound. As for $CoFe_2O_4$, $C_{v,Co}$, $C_{v,Fe}$ and $C_{v,O}$ are 24.81, 25.10 and 16.70 $J\cdot mol^{-1}\cdot K^{-1}$, respectively. The calculated value of specific heat capacity of $CoFe_2O_4$ is 141.81 $J\cdot mol^{-1}\cdot K^{-1}$.

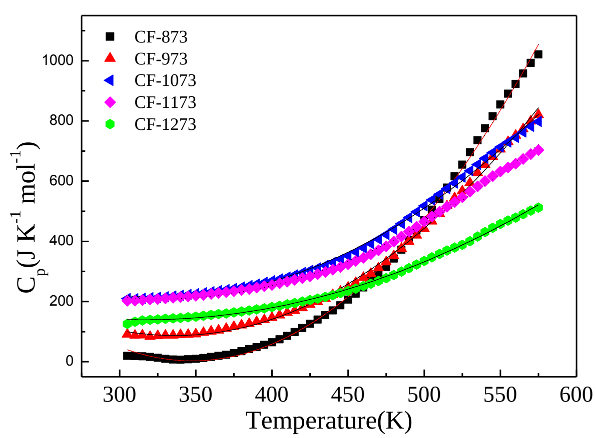

Figure 6. Molar heat capacity of $CoFe_2O_4$ microtubes as a function of temperature.

Insert Figure 6 here

Insert Table 4 here.

Table 4. Fitting paramours for Eq. 7

Samples	A	B	$C\times 10^{-4}$	R^2
CF-873	2457 ± 54	-14.12±0.25	203.20 ± 2.83	0.998
CF-973	1586 ± 40	-8.92 ± 0.19	132.70± 2.13	0.998
CF-1073	1267 ± 41	-6.45 ± 0.19	98.60 ± 2.16	0.998
CF-1173	1105 ± 37	-5.48 ± 0.17	83.80 ± 1.95	0.997
CF-1273	710± 21	-3.61 ± 0.10	57.10 ± 1.13	0.997

3.6 Hysteresis loss and specific heating rate of $CoFe_2O_4$ microtubes

The hysteresis loss is proportional to the area between the two magnetization curves and it is an important factor in evaluating the performance of materials used as susceptors of RF field [44, 45]. The hysteresis loss can be approximated as a function of coercivity and saturation magnetization [18] (Eq. 9):

$$P = C_0 \cdot H_c \cdot M_s \qquad (9)$$

where C_0 is a constant, which shows the ratio of the actual hysteresis loss to that in the case in which the magnetization curves form a rectangle with edges of M_S and H_c. The calculated hysteresis loss (kJ/mol, $M_s \times H_c$) and Experimental hysteresis loss(P, kJ/mol) are listed in Table 5.

Insert Table 5 here

Table 5 Hysteresis loss and specific heating rate of $CoFe_2O_4$ microtubes

Samples	CF- 873	CF - 973	CF - 1073	CF - 1173	CF -1273
Calculated hysteresis loss (kJ·m^{-3}, $M_s \times H_c$)	66.9	84.83	94.9	76.7	60.8
Experimental hysteresis loss(P, kJ·m^{-3})*	50.8	66.2	70.8	59.4	47.4
Value of Co	0.76	0.78	0.75	0.77	0.78
Specific heating rate (K/(s·mg))**	0.246	0.293	0.267	0.230	0.179

* Integrated region lies between -5kOe -5kOe,

**A coil with 500Oe field are used to test the heating rate of samples

It can be seen that a good agreement is obtained between the predicted and experimental values of hysteresis loss in the whole temperature range, as the constant C_o hardly varied . A slightly wave of C_o may derives from the choice of boundary value during the integrated process. Also, it can be seen clearly that the higher the saturation magnetization and coercivity, the more heat is produced/cycle of the magnetization reversal process. However, the latter is only true if the external field magnitude can reach the saturation magnetization in the ferrites [11]. Therefore, although these magnetic materials could theoretically produce more heat, in practice there are technical restrictions imposed on the amplitude of the applied field. In this study, the amplitude of magnetic field inside the coil was limited to 500 Oe, therefore, the heating rate is proportional to the actual hysteresis loss inside the coil. The latter is proportional to the area enclosed between the two magnetization curves and two vertical lines corresponding to magnetic field intensity of - 500 and 500 Oe.

The experimental specific heating rate of $CoFe_2O_4$ microtubes calcined at different temperatures is listed in Table 5. It can be seen that the sample CF-973 exhibits the highest specific heating rate of 0.293

K/(s·mg), which is 1.5 times higher than that of sample CF-1273, also higher than that of CF-1073.

4. Conclusions

One dimensional $CoFe_2O_4$ microtubes with the length exceeding 50 μm and with high specific surface area and magnetic saturation have been successfully prepared by the template-assisted sol-gel method. The cobalt ferrite spinel was the main phase for all samples. As the calcination temperature increased, the diameter, specific surface area and coercivity of microtubes monotnously decreased while the average crystal size and saturation magnetization increased. When calcined at 1073 K, a porous cobalt ferrite microtubes with a diameter in the range from 2 to 2.5 μm and an aspect ratio above 20 were produced, which consisted of rather uniform particles with a size about 80 nm, the specific surface area and average crystal size were 46.5 $m^2 \cdot g^{-1}$ and 66.9 nm. The specific surface area in the microtubes was near 10 times higher than that in the cobalt ferrite nanoparticles obtained at same conditions. The highest saturation magnetization equaled to 81.2 emu/g when calcined at 1273K and the highest coercivity was 1208 Oe at 873 K. The heat capacity was obtained as a function of temperature, value of the microtubes calcined at 973 K was 140.81 $J \cdot mol^{-1} \cdot K^{-1}$ at 395K. The microtubed calcined at 973 K, demonstrated the highest specific heating rate of 0.293 K/(s·mg) in RF field of 295 kHz.

5. Acknowledgements

The financial support from Royal Academy of Engineering for research exchanges with China and India–Major Award (2011-2012), EPSRC and the Science and Technology Planning Project of Hunan Province, China (2012WK3023) and the European Research Council (project 279867, “RF-enhanced microprocessing for fine chemicals synthesis using catalysts supported on magnetic nanoparticles, RFMiFiCS”) is gratefully acknowledged.

References

[1] Boury B., Nair R.G., Samdarshi S.K., Makiabadia T., Mutina P.H., New Journal of Chemistry 36(2012)2196-2000.

[2] Vyacheslav F. Solovyov, Li-jun Wu, Martin W. Rupich, Srivatsan Sathyamurthy, Xiaoping Li, Qiang Li, Journal of Crystal Growth 408(2014) 107-111

[3] Asit Kumar Gain, Liangchi Zhang, Weidong Liu, Materials & Design 67(2015)136-144

[4] Kyung-Jun Hwang, Cheol-Ho Hwang, In-Hwa Lee, Taewoo Kim, Sungho Jin, Ju-Young Park, Biomass and Bioenergy 68 (2014) 62-66.

[5] Hongtao Wang, Shumin Zhang, Taiqi Liu, Chemistry World(China) 12 (2005) 52-56.

[6] Yanwen Ma, Chuanyin Xiong, Wen Huang, Jin Zhao, Xingao Li, Quli Fan, Wei Huang, Chinese Journal of Inorganic Chemistry 03 (2012) 546-550.

[7] Yong Zhao, JinZhai, ,Shuxin Tan, Lifang Wang, Lei Jiang, Dao ben Zhu, Nanotechnology17(2006) 2090–2097.

[8] M. Eshraghi, P. Kameli, Current Applied Physics 11 (2011) 476-481.

[9] F.A. Harraz, R.M. Mohamed, M.M. Rashad, Y.C. Wang, W. Sigmund , Ceramics International 40 (2014) 375–384.

[10] R. Benraba, H. Boukhlouf, A. Löfberg, A. Rubbens, R.-N. Vannier, E. BordesRichard, A. Barama, Journal of Natural Gas Chemistry 21 (2012) 595–604.

[11] T.K. Houlding, E.V. Rebrov, Green Processing and Synthesis 1 (2012) 19–32.

[12] P. Gao, E.V. Rebrov, T.M.W.G.M. Verhoeven, J.C. Schouten, R. Kleismit, G. Kozlowski, J. Cetnar, Z. Turgut, G. Subramanyam, Journal of applied physics 107 (2010) 044317:1-7.

[13] E.V. Rebrov, P. Gao, T.M.W.G.M. Verhoeven, J.C. Schouten, R. Kleismit, Z. Turgut, G. Kozlowski, Journal of Magnetism and Magnetic Materials, 323 (2011) 723–729.

[14] A. Ovenston, J.R. Walls, Journal of the Chemical Society Faraday Transactions 1: Physical Chemistry in Condensed Phases 79 (1983) 1073–1084.

[15] S.I. Al-Mayman, S.M. Al-Zahrani, Fuel Processing Technology 80 (2003) 169–182.

[16] P. Duquenne, A. Deltour, G. Lacoste, International Journal of Heat and Mass Transfer 36 (1993) 2473–2477.

[17] T.K. Houlding, K. Tchabanenko, M.T. Rahman, E.V. Rebrov, Organic and Biomolecular Chemistry 11 (2013) 4171–4177.

[18] P. Gao, X. Hua, V. Degirmenci, D. Rooney, M. Khraisheh, R. Pollard, R.M. Bowman, E. V. Rebrov, Journal of Magnetism and Magnetic Materials 2013; 48: 44-50

[19] Peng-zhao Gao, Bing Yan, Dong-yun Li, Xiaxia Gan, Ping Li, Wei Liu, Key Engineering Materials 633 (2015) 26-30.

[20] Mahboubeh Houshiara,, Fatemeh Zebhi, Zahra Jafari Razi, Ali Alidoust, Zohreh Askari, Journal of Magnetism and Magnetic Materials 371 (2014) 43–48.

[21] Vittorio Berbenni , Chiara Milanese, Giovanna Bruni, Amedeo Marini. The combined effect of mechanical and thermal energy on the solid-state formation of $NiFe_2O_4$ from the system $2NiCO_3{\cdot}3Ni(OH)_2{\cdot}4H_2O–FeC_2O_4{\cdot}2H_2O$[J]. Thermochimica Acta 469 (2008) 86–90.

[22] Stefan Loos , Daniel Gruner, Mahmoud Abdel-Hafiez, Jürgen Seidel, Regina Hüttl, Anja U.B. Wolter, Klaus Bohmhammel , Florian Mertens. Heat capacity (Cp) and entropy of olivine-type $LiFePO_4$ in the temperature range (2 to 773) K[J]. J. Chem. Thermodynamics 85 (2015) 77–85

[23] O. Hascholu, Shi Hai-rong, Song Zhi-qiang, Liu Yu-jiang, O. Tegus. Determination of specific-heat capacity of Gd by Differential scanning calorimetry method[J]. Journal of Inner Mongolia Normal University(nature Science Edition), 2011,40(6): 586-588

[24] Peng-zhao Gao, Dong-yun Li, Xiao-liang Zhang, Bing Yan, Yu-kun Sun, Linv Xu, Ruixue Ma, Journal of Hunan University (Nature Science)(China) 41(7)(2014) 50-55.

[25] RaghvendraSinghYadav, JaromirHavlica, MiroslavHnatko, Pavol Šajgalík, Cigáň Alexander, MartinPalou, EvaBartoníčková, MartinBoháč, Františka Frajkorová, Jiri Masilko, MartinZmrzlý, LukasKalina, MiroslavaHajdúchová, Vojtěch Enev. Magnetic properties of $Co_{1-x}Zn_xFe_2O_4$ spinel ferrite nanoparticles synthesized by starch-assisted sol–gel autocombustion method and its ball milling. Journal of Magnetism and Magnetic Materials 378(2015)190–199.

[26] Yuanyuan Liao. The Study of Micro-structure and Optical Properties of Cobalt Ferrite Material $CoFe_2O_4$[D]. East China Normal University, 2013.32

[27] P. Chandramohan, M. P. Srinivasan, S. Velmurugan, S. V. Narasimhan, Cation distribution and particle size effect on Raman spectrum of CoFe2O4, J. Solid State Chem.184(2011)89–96.

[28] Z. Wang, P. Lazor, S. K. Saxena, H .S. C. O'Neill, Mater.Res.Bull.37(9)(2002) 1589–1602.

[29] Yuqiu Qu, Haibin Yang, Nan Yang, Yuzun Fan, Hongyang Zhu, Guangtian Zou. The effect of reaction temperature on the particle size, structure and magnetic properties of coprecipitated $CoFe_2O_4$ nanoparticles. Materials Letters 60 (2006) 3548-3552.

[30] Lu A H, Salabas E L and Schüth F , Angew. Chem. Int. Edn Engl. 2007, 46, 1222-1244

[31] A.L. Xia, C.H. Zuo, L.J. Zhang, C.X. Cao, Y. Deng, W. Xu, M.F. Xie, S.L. Ran, C.G. Jin, X.G. Liu, Journal of physics D-applied physics 47 (2014) 415004.

[32] M.A. Gabal, Journal of Magnetism and Magnetic Materials 321 (2009) 3144–3148.

[33] M. Younas, M. Atif, M. Nadeem, M. Siddique, M. Idrees, R. Grossinger, Journal of Physics D: Applied Physics 44 (2011) 345402.

[34] Bao Huang. Synthesis and magnetic properties of nanostructure magnetic cobalt ferrites[D]. China Jiliang University, 2014, 6 35-36

[35] K. Maaz, S. Karim, A. Mumtaz, S.K. Hasanain, J. Liu, J.L. Duan, Journal of Magnetism and Magnetic Materials 321(2009) 1838–1842.

[36] Sunghyun Yoon, Journal of Magnetism and Magnetic Materials 324 (2012) 2620–2624

[37] I.Z. Rahman, T.T. Ahmed, Journal of Magnetism and Magnetic Materials 290–291 (2)(2005) 1576–1579

[38] Z. Peng, X. Fu, H. Ge, Z. Fu, C. Wang, L. Qi, H. Miao, Journal of Magnetism and Magnetic Materials 323 (2011) 2513–2518.

[39] Yue Zhang, Zhi Yang, Di Yin, Yong Liu, ChunLong Fei, Rui Xiong, Jing Shi, GaoLin Yan, Journal of Magnetism and Magnetic Materials 322 (2010) 3470–3475.

[40] B.D. Cullity. Elements of X-ray Diffraction, Addison-Wesly Publishing Co. Inc. 1976 (Chapter 14).

[41] Xue D.S., Chai G.Z., Li X.L., Fan X. L. , Journal of Magnetism and Magnetic Materials 320(2008)1541–1543.

[42] Qian Ma. Study on the preparation and magnetic properties of $Ni_{1-x}Zn_xFe_2O_4$ nanoparticles and composite with Co_3O_4[D]. Anhui University (China), 2013, 23-25.

[43] M.M. Efremova, A.A. Popova, A.S. Monayenkova, L.A. , Journal of Alloys and Compounds 452(2008) 99-101

[44] S. Chatterjee, V. Degirmenci, F. Aiouache, E.V. Rebrov Design of a radio frequency heated isothermal micro-trickle bed reactor. Chem Eng J 2014; 243: 225–233.

[45] Thomas K. Houlding, Pengzhao Gao, Volkan Degirmenci, Kirill Tchabanenko, Evgeny V. Rebrov, Mechanochemical synthesis of $TiO_2/NiFe_2O_4$ magnetic catalysts for operation under RF field, Materials Science and Engineering: B 193(2015) 175-180.

[46] Zheng-lie Wang, Ya-ping Zhou. Physics chemistry [M], High education press (China, Beijing), 2001,12, 310